Enhanced Second-Harmonic Generation by Metal Surfaces with Nanoscale Roughness: Nanoscale Dephasing, Depolarization, and Correlations

Mark I. Stockman,[1,*] David J. Bergman,[2,†] Cristelle Anceau,[3] Sophie Brasselet,[3,‡] and Joseph Zyss[3,§]

[1]*Department of Physics and Astronomy, Georgia State University, Atlanta, Georgia, 30303, USA*

[2]*School of Physics and Astronomy, Raymond and Beverly Sackler Faculty of Exact Sciences, Tel Aviv University, Tel Aviv, 69978, Israel*

[3]*Laboratoire de Photonique Quantique et Moléculaire, Ecole Normale Supérieure de Cachan, 94235 Cachan, France*

(Received 25 July 2003; published 6 February 2004)

On the basis of spectral-expansion Green's function theory, we theoretically describe the topography, polarization, and spatial-coherence properties of the second-harmonic (SH) local fields at rough metal surfaces. The spatial distributions of the fundamental frequency and SH local fields are very different, with highly enhanced hot spots of the SH. The spatial correlation functions of the amplitude, phase, and direction of the SH polarization all show spatial decay on the nanoscale in the wide range of the metal fill factors. This implies that SH radiation collected from even nanometer-scale areas is strongly depolarized and dephased, i.e., has the nature of hyper-Rayleigh scattering, in agreement with recent experiments. The present theory is applicable to nanometer-scale nonlinear-optical illumination, probing, and modification.

DOI: 10.1103/PhysRevLett.92.057402 PACS numbers: 78.67.–n, 68.37.Uv, 73.20.Mf

There has recently been great interest in optical properties of metallic nanostructures, in particular, nanorough metal surfaces and clusters. The giant fluctuations and enhancement of local fields in such resonant random systems lead to the corresponding giant enhancement of two- and many-photon processes [1]. This has been especially well studied for surface-enhanced Raman scattering (SERS) [2]. The record enhancement of SERS, $\gtrsim 10^{12}$, allowed for Raman observation of single molecules [3,4]. Second-harmonic generation (SHG) in systems built of isotropic metals is principally different from SERS in two respects. First, SHG is a coherent process implying the interference of waves emitted by different sites; therefore, dephasing of the second-harmonic (SH) polarization is of importance. This dephasing is the randomization of the SH-polarization phase in the plane of the nanostructure due to the spectral detuning of localized eigenmodes from the excitation frequency. Second, the SHG is a second-order (three-wave) process where for a center-symmetric medium, the SH polarization is concentrated at surfaces and interfaces, while the bulk contribution is suppressed. This is in contrast to odd-order processes such as the phase conjugation where the coherent generation of radiation and giant enhancement were observed [5].

The recent experimental study of SHG by rough gold surfaces with the spatial resolution of 400 nm [6] revealed intriguing properties of SHG: (i) SHG is incoherent, i.e., hyper-Rayleigh scattering, implying strong dephasing. (ii) SHG is almost completely depolarized despite the small detection area. (iii) The SHG has a topography of localized bright "hot spots." This topography and depolarization were independently supported and the enhancement of SHG in the hot spots up to 3 orders of magnitude was found [7]. This Letter establishes theoretically that the dephasing and depolarization for SH originate at the minimum scale of the system, on the order of a few nanometers implying SHG on nanorough metal surfaces to be a depolarized hyper-Rayleigh scattering.

Because the phenomena to be discussed originate at the nanoscale, we consider a nanosystem whose entire extent is much smaller than the light wavelength and use the quasistatic approximation. The rough surface is described by the local dielectric function $\varepsilon(\mathbf{r}, \omega) = \varepsilon(\omega)\Theta(\mathbf{r}) + \varepsilon_h[1 - \Theta(\mathbf{r})]$ depending on coordinate $\mathbf{r}$ and excitation frequency ω, where $\varepsilon(\omega)$ is the dielectric function of the metal, ε_h is the permittivity of the dielectric host, and $\Theta(\mathbf{r})$ is the characteristic function equal to 1 for $\mathbf{r}$ inside the metal component and 0 otherwise.

The expression for the linear electric potential at the fundamental frequency ω is

$$\varphi(\mathbf{r}) = \varphi_0(\mathbf{r}) - \int \varphi_0(\mathbf{r}')\nabla'^2 G^r(\mathbf{r}, \mathbf{r}'; \omega) d^3 r', \qquad (1)$$

where $\varphi_0(\mathbf{r})$ is the external excitation potential, and $G^r(\mathbf{r}, \mathbf{r}'; \omega)$ is the retarded Green's function [8,9].

Consider the form of the SH nonlinear polarization $\mathbf{P}_{\mathrm{NL}}^{(2)}$. In an isotropic medium, it contains three terms originating in the bulk of the metal [10]:

$$\mathbf{P}_{\mathrm{NL}}^{(2)} = \alpha\Theta\mathbf{E}(\nabla \cdot \mathbf{E}) + \beta\Theta(\mathbf{E} \cdot \nabla)\mathbf{E} + \gamma\Theta\mathbf{E} \times [\nabla \times \mathbf{E}], \qquad (2)$$

where $\Theta = \Theta(\mathbf{r})$, $\mathbf{E} = -\nabla\varphi$, and α, β, and γ are scalar functions of ω (coefficients of the SH hyperpolarizability). Likewise, there are three surface contributions:

$$\mathbf{P}_{\mathrm{NL}}^{(2)} = A\mathbf{E}(\mathbf{E} \cdot \nabla\Theta) + B\mathbf{E}^2\nabla\Theta + C\mathbf{E} \times [\nabla\Theta \times \mathbf{E}]. \qquad (3)$$

The last term in Eq. (2) vanishes in the quasistatic approximation. We assume a good metal for which in the optical region $|\varepsilon(\omega)| \gg 1$. Then the fields inside the

metal are small as well as their tangential components at the surfaces. Resultantly, the α, β, A, and B terms in Eqs. (2) and (3) are equivalent, and the C term can be neglected. Therefore, assuming a good metal, without sacrificing the generality of our theory, we can set, e.g.,

$$\mathbf{P}_{\mathrm{NL}}^{(2)}(\mathbf{r}) = B\mathbf{E}^2(\mathbf{r})\nabla\Theta(\mathbf{r}). \quad (4)$$

Here, nonlinear polarizability B determines only the magnitude of the SHG but vanishes from the polarization, spatial coherence, or relative SHG enhancement.

The SH (second-order) field potential induced due to polarization (4) can be calculated as a contraction

$$\varphi^{(2)}(\mathbf{r}) = -\frac{4\pi}{\varepsilon_h}\int \bar{G}^r(\mathbf{r}, \mathbf{r}'; 2\omega)\nabla' \cdot \mathbf{P}_{\mathrm{NL}}^{(2)}(\mathbf{r}')d^3r'. \quad (5)$$

Here $\bar{G}^r(\mathbf{r}, \mathbf{r}')$ is a retarded Green's function, different from $G^r(\mathbf{r}, \mathbf{r}')$ of Ref. [9], which is given by the following spectral expansion over the eigenmodes of the system:

$$\bar{G}^r(\mathbf{r}, \mathbf{r}'; \omega) = \sum_n \phi_n(\mathbf{r})\phi_n^*(\mathbf{r}')/[s(\omega) - s_n], \quad (6)$$

where $s(\omega) = \varepsilon_h/[\varepsilon_h - \varepsilon(\omega)]$ is the spectral parameter [11], and $\phi_n(\mathbf{r})$ and s_n are the eigenfunctions and eigenvalues of the surface plasmon (SP) eigenproblem [8]. The Green's function approach is highly stable numerically.

The SH electric field, $\mathbf{E}^{(2)}(\mathbf{r}) = -\nabla\varphi^{(2)}(\mathbf{r})$, in turn induces a contribution to the SH polarization due to the linear polarizability at the SH frequency of 2ω. Resultantly, the total SH polarization is computed as

$$\mathbf{P}^{(2)}(\mathbf{r}) = \mathbf{P}_{\mathrm{NL}}^{(2)}(\mathbf{r}) + \mathbf{E}^{(2)}(\mathbf{r})[\varepsilon(\mathbf{r}, 2\omega) - 1]/(4\pi). \quad (7)$$

We solved the eigenproblem numerically as described in Ref. [8]. For statistical averaging, we employed ensembles of 64 systems of each kind. Every system was a random planar composite (RPC) in the space of $32 \times 8 \times 32$ grid steps; to check the accuracy, we carried out some computations with $32 \times 16 \times 32$ and $32 \times 32 \times 32$ grids. We set the excitation field to be unity ($E_0 = 1$) and z polarized.

An example of RPC geometry is illustrated in Fig. 1(a) where $\Theta(\mathbf{r})$ is displayed in the plane of the RPC. To regularize the underlying partial differential equations, as in Ref. [8], we smooth $\Theta(\mathbf{r})$ by applying a Gaussian filter with the width of one grid step; this greatly improves the convergence with decreasing the grid step.

The local electric field $\mathbf{E}(\mathbf{r})$ in the plane of such an RPC made of silver calculated from Eq. (1) using the data of Ref. [12] is shown in Fig. 1(b). One can see a set of hot spots that are much more densely distributed, and the overall distribution is significantly delocalized compared with fractal composites [13]. The maximum field $E = 35$ is in agreement with an estimate based on the quality factor of a SP resonance, $E \sim \mathrm{Re}\varepsilon/\mathrm{Im}\varepsilon \sim 30$.

The SH polarization $\mathbf{P}^{(2)}(\mathbf{r})$ displayed in Fig. 1(c) is qualitatively different: the number of hot spots is significantly smaller, and their magnitudes do not correlate appreciably with those in panel (b); the SH hot spots

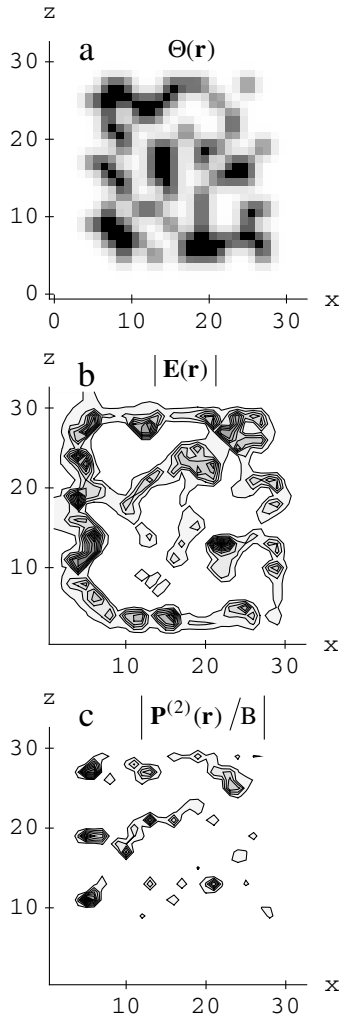

FIG. 1. (a) Geometry of random planar composite (cross section through the plane of symmetry): characteristic function $\Theta(\mathbf{r})$ displayed as a density plot. The axis unit is the grid step; one unit may correspond to a length between 2 and 5 nm. Fill factor $p = 0.5$. (b) Spatial distribution of the magnitude of the local linear field, $|\mathbf{E}(\mathbf{r})|$, in the plane of the RPC shown as a contour map; $\max|\mathbf{E}| = 35$. (c) Same as (b) but for the SH polarization enhancement, $|\mathbf{P}^{(2)}(\mathbf{r})/B|$; $\max|\mathbf{P}^{(2)}/B| = 250$.

are pronounced only at positions of the fundamental-harmonic hot spots, but only of some of them. These data are qualitatively consistent with the inference of Ref. [7] that SHG occurs at sites where the fundamental and SH modes spatially overlap. The hot spots of SHG occur at those linear field sites where random fluctuations of the RPC cause non-center-symmetric local configurations. Quantitatively, though SHG is enhanced by the maximum factor of up to 250, the magnitude $|\mathbf{P}^{(2)}(\mathbf{r})|$ is still significantly smaller than $|\mathbf{E}(\mathbf{r})|^2 \lesssim 10^3$, which implies that the SHG is significantly suppressed.

Further insight into the physical cause of the observed depolarization can be obtained from Fig. 2 where the SH-polarization vector $\mathbf{P}^{(2)}(\mathbf{r})$ is plotted for each grid cell of the system. The most striking feature manifest in this figure is that both $\mathrm{Re}\mathbf{P}^{(2)}(\mathbf{r})$ and $\mathrm{Im}\mathbf{P}^{(2)}(\mathbf{r})$ are strongly

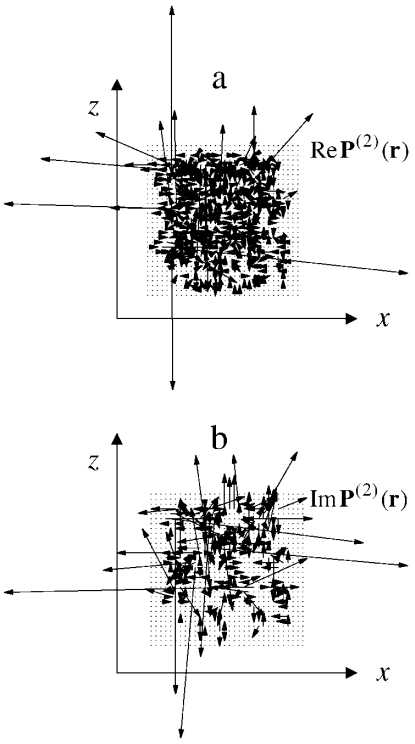

FIG. 2. (a) Vector-field plot of the real part of the total SH polarization, $\mathrm{Re}\mathbf{P}^{(2)}(\mathbf{r})$: for every point $\mathbf{r}$ of the RPC, $\mathrm{Re}\mathbf{P}^{(2)}(\mathbf{r})$ is shown as an arrow beginning at that point. If $\mathrm{Re}\mathbf{P}^{(2)}(\mathbf{r})$ is essentially zero, it is shown as a dot. (b) The same for $\mathrm{Im}\mathbf{P}^{(2)}(\mathbf{r})$.

depolarized: the polarization vectors are randomly oriented. It is also obvious that very close points may have very differently directed $\mathbf{P}^{(2)}(\mathbf{r})$; this suggests that the depolarization originates at the minimum scale.

The origin of the dephasing can be inferred from Fig. 3 where the SH phase is represented by the polar angle. Note that the black blobs in this figure correspond to the regions of the space where $|\mathbf{P}^{(2)}|$ is very small (the phase singularity), e.g., in the host. The vector trajectory forms a closed loop for the spatial points corresponding to the crossing of a resonance location (hot spot). There is ample evidence of such loops in Fig. 3. As a result of these resonances, the phase curve trajectory resembles diffusion, and the directional (i.e., phase) memory is lost; hence, there is strong dephasing.

The quantitative information on the dephasing and depolarization is contained in the corresponding correlation functions. The amplitude correlator is sensitive to both the depolarization and dephasing:

$$C(\mathbf{r}) = \mathrm{Re}\left\langle \int \mathbf{P}^{(2)}(\mathbf{r}_1) \cdot \mathbf{P}^{(2)*}(\mathbf{r}_1 - \mathbf{r}) d^3 r_1 \right\rangle, \quad (8)$$

where the angular brackets denote the statistical averaging. The absolute phase of the SH polarization ϕ is defined as $e^{i2\phi} = \mathbf{P}^{(2)2}/|\mathbf{P}^{(2)}|^2$. Hence, the following correlation function is sensitive to only the dephasing, but not the polarization direction:

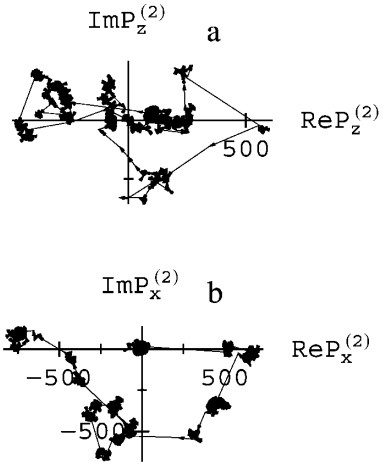

FIG. 3. (a) Phase plane plot of $P_z^{(2)}(\mathbf{r})$ (the component polarized in the direction of the exciting field). For each grid cell of the system, we plot $\mathrm{Im}P_z^{(2)}(\mathbf{r})$ against $\mathrm{Re}P_z^{(2)}(\mathbf{r})$ starting from the sum of the previously plotted vectors. (b) Similar plot for $P_x^{(2)}(\mathbf{r})$ (the depolarized component).

$$C_{\mathrm{phase}}(\mathbf{r}) = \mathrm{Re}\left\langle \int \sqrt{\mathbf{P}^{(2)2}(\mathbf{r}_1)\mathbf{P}^{(2)2*}(\mathbf{r}_1 - \mathbf{r})}\, d^3 r_1 \right\rangle. \quad (9)$$

To define the directional correlation function, we introduce the SH-polarization density matrix $\rho_{ij}(\mathbf{r}) = \mathrm{Re}[P_i^{(2)}(\mathbf{r})P_j^{(2)}(\mathbf{r})^*]$, where $i, j = x, z$, and light is assumed to be incident along the y axis. The eigenvalues of this matrix are $\rho_\pm = \frac{1}{2}\{\rho_{xx} - \rho_{zz} \pm \sqrt{[\rho_{xx} - \rho_{zz}]^2 + 4\rho_{xz}}\}$. The angle between the ellipse major axis and the x axis is $\theta = -\arctan(2\rho_{xz}/\rho_+)$. The polarization-direction correlator is defined as

$$C_{\mathrm{polariz}}(\mathbf{r}) = \left\langle \int \cos[\theta(\mathbf{r}_1) - \theta(\mathbf{r}_1 - \mathbf{r})] \times \sqrt{\rho_+(\mathbf{r}_1)\,\rho_+(\mathbf{r}_1 - \mathbf{r})}\, d^3 r_1 \right\rangle. \quad (10)$$

It is selectively sensitive to the polarization direction, but not to the dephasing.

These spatial correlation functions are displayed in Fig. 4. Amplitude-correlation function $C(r)$ [Fig. 4(a)] shows the decay at the minimum scale ($r \approx 1$) irrespective of fill factor p. This alone implies that SHG is incoherent down to a minimum scale. At the highest fill factor of $p = 0.95$, $C(r)$ oscillates with the period commensurate with the total size of the system. This feature is an artifact due to the finite system size in our simulations where the standing SP wave is formed caused by the reflections from its boundaries; in experiments, it may be quite different due to the much larger size of the system.

Phase-correlation function $C_{\mathrm{phase}}(r)$ [Fig. 4(b)] exhibits a decay whose radius r increases monotonously with p but still is on the nanoscale. This implies a role of the delocalization of eigenmodes [8] in the dephasing. The SH

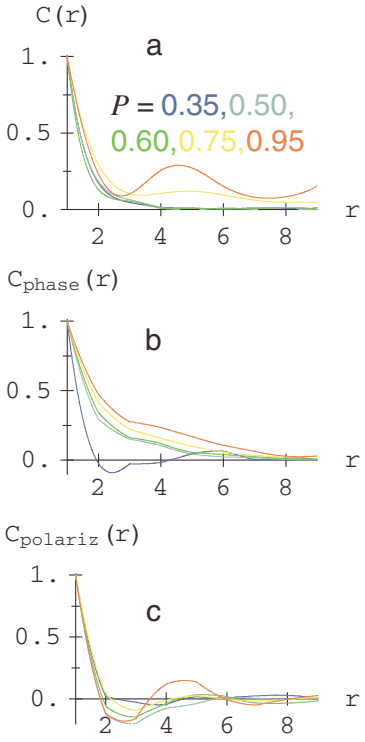

FIG. 4 (color). The correlation functions of the SH polarization (normalized to 1 for $r = 0$) vs radius r for different fill factors p (color coded). (a) Amplitude correlation function $C(r)$ computed from Eq. (8). The color-coded values of p are indicated. (b) Phase correlation function C_{phase} computed from Eq. (9). (c) Polarization-direction correlation function C_{polariz} computed from Eq. (10).

phase stays constant within a hot spot whose radius increases with p. Dephasing occurs when the hot spots of two eigenmodes with randomly differing frequencies overlap due to their delocalization. In such a case, the strong local field of one of those eigenmodes induces the oscillations of the other with the random phase shift that, depending on their spectral detuning, can change from 0 to π. In contrast, the behavior of the polarization-correlation function [Fig. 4(c)] is similar to that of the amplitude correlator $C(r)$ [cf. Fig. 4(a)]. This implies that the depolarization of the SHG originates at the minimum scale of the system, and it is complete at the scale of several nanometers. This can be understood from the fact that for a good metal, $\mathbf{P}^{(2)}$ is generated at the surfaces in the normal directions; the randomness of the RPC surface at the minimum scale is responsible for the depolarization (the random orientation of $\mathbf{P}^{(2)}$). By averaging, we have also found that Stokes's degree of polarization for the entire structure is very low, $\sim 10\%$.

To briefly summarize, we have shown theoretically that SH local fields for nanorough metal surfaces are singular on the nanoscale, forming SH hot spots where the local SH fields are enhanced by more than 2 orders of magnitude. The SH local fields at the nanoscale are both strongly depolarized and dephased. This implies, in particular, the incoherent nature of SHG as the hyper-Rayleigh scattering that persists even for the smallest areas resolved. These findings are in accord with the recent experiments [6,7]. They have direct significance for applications involving nanomodification or probing at nanoscale using the surface-enhanced SH fields. In particular, the depolarized and incoherent SH fields may have unique advantages for illumination on the nanoscale.

This work was supported by the Chemical Sciences, Biosciences and Geosciences Division of the Office of Basic Energy Sciences, Office of Science, U.S. Department of Energy, and the U.S.-Israel Binational Science Foundation, and the Israel Science Foundation.

*Electronic address: mstockman@gsu.edu
URL: http://www.phy-astr.gsu.edu/stockman
†Electronic address: bergman@post.tau.ac.il
‡Electronic address: sophie.brasselet@lpqm.ens-cachan.fr
§Electronic address: zyss@lpqm.ens-cachan.fr

[1] M. I. Stockman, L. N. Pandey, L. S. Muratov, and T. F. George, Phys. Rev. Lett. **72**, 2486 (1994).
[2] M. Moskovits, Rev. Mod. Phys. **57**, 783 (1985).
[3] K. Kneipp, Y. Wang, H. Kneipp, L. T. Perelman, I. Itzkan, R. R. Dasari, and M. S. Feld, Phys. Rev. Lett. **78**, 1667 (1997).
[4] S. Nie and S. R. Emory, Science **275**, 1102 (1997).
[5] S. G. Rautian, V. P. Safonov, P. A. Chubakov, V. M. Shalaev, and M. I. Stockman, Pis'ma Zh. Eksp. Teor. Fiz. **47**, 200 (1988) [JETP Lett. **47**, 243 (1988)].
[6] C. Anceau, S. Brasselet, J. Zyss, and P. Gadenne, Opt. Lett. **28**, 713 (2003).
[7] S. I. Bozhevolnyi, J. Beermann, and V. Coello, Phys. Rev. Lett. **90**, 197403 (2003).
[8] M. I. Stockman, S.V. Faleev, and D. J. Bergman, Phys. Rev. Lett. **87**, 167401 (2001).
[9] M. I. Stockman, S.V. Faleev, and D. J. Bergman, Phys. Rev. Lett. **88**, 067402 (2002).
[10] C. K. Chen, T. F. Heinz, D. Ricard, and Y. R. Shen, Phys. Rev. B **27**, 1965 (1983).
[11] D. J. Bergman and D. Stroud, in *Solid State Physics*, edited by H. Ehrenreich and D. Turnbull (Academic Press, Boston, 1992), Vol. 46, pp. 148–270.
[12] P. B. Johnson and R.W. Christy, Phys. Rev. B **6**, 4370 (1972).
[13] M. I. Stockman, L. N. Pandey, and T. F. George, Phys. Rev. B **53**, 2183 (1996).